Early life changes in histone landscape protect against age-associated amyloid toxicities through HSF-1 dependent regulation of lipid metabolism

Ursula Jakob (ujakob@umich.edu)
University of Michigan
Bryndon Oleson
University of Michigan
Janakraj Bhattrai
University of Michigan
Sarah Zalubas
University of Michigan
Tessa Kravchenko
University of Michigan
Yuanyuan Ji
University of Maryland School of Pharmacy
Emily Jiang
University of Michigan https://orcid.org/0009-0003-5353-6474
Christine Lu
University of Michigan
Ciara Madden
University of Michigan
Daphne Bazopoulou
University of Crete
Jace Jones
University of Maryland School of Pharmacy

Article

Keywords:

Posted Date: April 20th, 2023

DOI: https://doi.org/10.21203/rs.3.rs-2782739/v1

Additional Declarations: There is **NO** Competing Interest.

Early life changes in histone landscape protect against age-associated amyloid toxicities through HSF-1 dependent regulation of lipid metabolism

Bryndon J. Oleson[1], Janakraj Bhattrai[1], Sarah L. Zalubas[1], Tessa R. Kravchenko[1], Yuanyuan Ji[3], Emily Jiang[1], Christine C. Lu[1], Ciara R. Madden[1], Daphne Bazopoulou[1,2], Jace W. Jones[3], Ursula Jakob[1, 4*]

[1]Department of Molecular, Cellular, and Developmental Biology, University of Michigan, Ann Arbor, MI, USA

[2]Current Address: Dept. of Biology, University of Crete, Heraklion, Greece

[3]Department of Pharmaceutical Sciences, University of Maryland School of Pharmacy, Baltimore, MD, USA

[4]Biological Chemistry Department, University of Michigan Medical School, Ann Arbor, USA

*Corresponding author

Phone: +1-734-615-1286

Email: ujakob@umich.edu

Abstract

Recent studies revealed that early-in-life events can have highly beneficial long-term effects in animals. We now demonstrate that exposure of *Caenorhabditis elegans* to reactive oxygen species during development protects against amyloid-induced proteotoxicity later in life. We show that this protection is initiated by the inactivation of the redox sensitive H3K4me3 modifying COMPASS complex, and conferred by a substantial increase in the heat shock independent activity of heat shock factor 1 (HSF-1), a longevity factor known to act predominantly during *C. elegans* development. We show that depletion of HSF-1 leads to dramatic rearrangements of the organismal lipid landscape, and a significant decrease in mitochondrial β-oxidation. Both of these activities appear to majorly contribute to HSF-1's protective effects against amyloid toxicity. In summary, our study reveals previously unknown links between developmental changes in the histone landscape, HSF-1 activity and lipid metabolism and the protection against age-associated amyloid toxicities later in life.

Introduction

Many biological processes contain seemingly stochastic components that cannot be explained by genetic or environmental variations[1,2]. This noise in the system becomes particularly obvious in synchronized populations of isogenic organisms, such as *Caenorhabditis elegans*, which show dramatic inter-individual differences in their lifespans as well as their susceptibility towards amyloid-mediated proteotoxicity[2–5]. Recent studies in *C. elegans* strains equipped with chromosomally encoded ratiometric *in vivo* redox sensors revealed that naturally occurring variations in the levels of reactive oxygen species (ROS) during early development are responsible for some of the observed lifespan variations[6,7]. Analysis of worms sorted according to their early life redox states showed that the most oxidized animals in the L2 larval stage are significantly more stress resistant and develop into more reduced and longer-lived animals than their oxidized counterparts[6,7]. These results suggested that naturally occurring early-in-life events exist which can significantly improve health and lifespan. Similar beneficial early-in-life events have also recently been reported for mice, where food reduction in pre-weaning mice or rapamycin treatment for the first 4 weeks after birth were found to be sufficient to extend lifespan up to 15%[8,9]. Mechanistic follow-up studies in *C. elegans* revealed that the highly conserved methyltransferase SET-2, the central component of the H3K4me3-depositing COMPASS complex[10], is redox sensitive, and its reversible inactivation responsible for a substantial reduction in global H3K4me3 levels in the oxidized subpopulation of *C. elegans*[7]. Genetic downregulation of members of the COMPASS complex, including SET-2 and ASH-2 increased heat shock and oxidative stress resistance and substantially extended lifespan, essentially phenocopying the oxidized subpopulation[7,11]. Earlier studies in *C. elegans*, which showed that H3K4me3 is deposited on transcriptional start sites before the L3 larval stage[12], helped to explain how a transient ROS-mediated event during development can exert these long-lasting effects.

Age is the greatest non-genetic risk factor for neurodegenerative diseases such as Alzheimer's disease (AD) or Huntington's disease (HD)[13]. These diseases manifest through the deposition of amyloidogenic proteins, including the $A\beta_{1-42}$-peptide, Tau or polyglutamine (polyQ) expansion proteins, as insoluble fibrils and plaques[13–16]. Lifespan-extending interventions have recently been shown to protect against amyloid-associated proteotoxicity in a variety of model organisms[17–21], suggesting that aging pathways may be suitable targets for preventing or treating age-associated neurodegenerative diseases. In this study, we explored if and how early-in-life events that expand lifespan protect organisms against amyloid-associated proteotoxicity later in life. We discovered that the transient exposure of *C. elegans* to ROS in early life significantly delays the onset of amyloid toxicity in a COMPASS complex-dependent manner, and demonstrated that the genetic or pharmacological depletion of members of the COMPASS complex (i.e., *ash-2*, *set-2*) protects a range of different *C. elegans* strains against $A\beta_{1-42}$ and polyQ-mediated toxicities. Mechanistic follow-up studies revealed that the depletion of members of the COMPASS complex causes a significant functional upregulation of the heat shock factor 1 (HSF-1), a conserved longevity factor previously shown to act predominantly during early life stages of *C. elegans*[18,22–24]. Unexpectedly, we found that HSF-1's protective effect is largely unrelated to its known role in regulating the expression of members of the cellular proteostasis network. Instead, we discovered that increasing the activity of HSF-1 in early life significantly alters several aspects of *C. elegans'* lipid homeostasis, previously associated with lifespan extension[25]. These changes include an increase of short-chain fatty acids, an increase in monounsaturated fatty acids (MUFAs), and an upregulation of mitochondrial β-oxidation. Our studies thus reveal a previously unknown connection between early-in-life changes in the histone landscape, heat shock *in*dependent HSF-1 activity, altered lipid metabolism and the protection against age-associated amyloid toxicities later in life.

Results

Early-in-life ROS exposure protects C. elegans against amyloid toxicity later in life

Our previous work in *C. elegans* demonstrated that transiently elevated levels of ROS during early development, either naturally produced or exogenously applied in the form of paraquat (PQ), extend lifespan through the oxidative inactivation of the COMPASS complex[7]. To test the intriguing idea that early life oxidative stress might protect organisms against amyloid-induced toxicity later in life, we exposed a *C. elegans* mutant strain, which expresses the human $A\beta_{1-42}$ peptide in its body wall muscle cells (i.e., strain CL4176), to a transient 10-h paraquat treatment during early development followed by a shift in temperature to induce $A\beta_{1-42}$ expression (Fig. 1A). As shown before, these worms get prematurely paralyzed as the levels of amyloids and amyloidogenic aggregates increase (Fig. 1B, black trace)[26]. Short-term exposure to the ROS-generating compound paraquat (PQ), however, significantly delayed this onset of paralysis (Fig. 1B, black dashed trace), providing first evidence that transient, early-in-life events might be able to protect organisms against proteotoxicity elicited by amyloidogenic proteins at later stage in life. To test whether this protective effect is mediated by the oxidative downregulation of the COMPASS complex, we crossed the CL4176 strain with a *C. elegans* mutant strain lacking *set-2*, the redox sensitive component of the COMPASS complex[7]. Movement analysis revealed that the *set-2* deletion strain showed a delay in the onset of paralysis that was similar to PQ-treated CL4176 and no longer responsive to PQ treatment (Fig. 1B, compare green solid and dashed traces). These results excluded any PQ-specific effects on $A\beta_{1-42}$ expression or toxicity. Instead, they indicated that the protective effects of the transient exposure to ROS in early life are likely mediated by the oxidative stress-induced inactivation of members of the COMPASS complex.

Depletion of H3K4me3 modifiers widely protects C. elegans against amyloid-related proteotoxicity

Recent studies in mouse models of Alzheimer's disease revealed that the pharmacological inhibition of the mammalian COMPASS complex significantly improved memory deficits in mouse models of Alzheimer's disease[19]. We now found that the addition of the SET-2 inhibitor MM-401[27] protects $A\beta_{1-42}$ expressing CL4176 worms against premature paralysis (Fig. 1C). The observed delay in paralysis was comparable to *C. elegans* strains either transiently treated with PQ during development (Fig. 1B) or grown on RNAi bacteria targeting *ash-2* or *set-2* (Fig. 1D). These results supported our conclusion that inactivation of the COMPASS complex, either through oxidative stress, genetic depletion or pharmacological intervention, protects organisms against amyloid-mediated toxicity. To investigate whether a reduction in the functional activity of the COMPASS complex protects *C. elegans* more generally against amyloid-induced proteotoxicity, we tested a number of additional, previously established *C. elegans* models for amyloid toxicity; CL2006, which chronically expresses the human $A\beta_{1-42}$ peptide in the body wall muscle and experiences toxicity and displays premature paralysis later in life[26,28,29]; GRU102, which expresses the human $A\beta_{1-42}$ peptide pan-neuronally and dies prematurely[30]; and AM141, a strain that expresses a highly amyloidogenic 40-residue glutamine tract (Q40) fused to Yellow Fluorescent Protein (YFP)[31]. This strain accumulates visible foci at the onset of adulthood and displays signs of paralysis about three to five days later. We prepared synchronized populations for each of these strains and maintained them on the control bacteria RNAi strain L4440 or on RNAi strains that either target *ash-2* or *set-2*, which reproducibly reduce global H3K4me3 levels by about 50% (inserts in Fig. 1D, E, G). Paralysis and lifespan analysis revealed that the animals deficient in either *ash-2* or *set-2* are significantly protected from proteotoxicity compared to the isogenic strains grown on control RNAi, independent of the timing of expression, i.e., acute *versus* chronic $A\beta_{1-42}$ toxicity (Fig. 1 D, E), the tissues in which the amyloidogenic proteins are expressed, *i.e.,* muscle *versus* neurons (Fig. 1E, F), or the types of amyloidogenic proteins expressed, *i.e.* $A\beta_{1-42}$ *versus* Q40::YFP (Fig. 1E, G) (Table S1). The protective effects of the *ash-2* depletion were overall more

robust and reproducible than the effects of the *set-2* depletion, an observation that was in line with their respective effects on *C. elegans* lifespan[11]. It is of note that the knockdown of members of the COMPASS complex neither altered the ratio of monomeric to higher oligomeric $A\beta_{1-42}$ species nor the steady state levels of either amyloidogenic protein (Fig. S1A-D), indicating that the protective effects associated with the reduction in COMPASS complex activity are not caused by a reduction in the levels of toxic proteins. In fact, analysis of the number of visible foci in day-1 old Q40::YFP expressing adults revealed an increase in aggregate formation in worms either maintained on *ash-2* or *set-2* RNAi (Fig. S1E, F) or crossed with a *set-2(ok952)* deletion mutant (Fig. S1G, H) relative to the control animals. While the latter results are initially counterintuitive, they are consistent with several more recent studies, which showed that not the quantity but the quality and composition of protein aggregates correlate with their *in vivo* toxicity[32–34]. Based on these data, we thus concluded that the reduction in the functional activity of the COMPASS complex provides *C. elegans* with a widespread protection against amyloid-related toxicities.

Protective effects of H3K4me3 modifier depletion requires heat shock factor 1

Our earlier studies revealed that the oxidative inactivation of H3K4me3 modifiers during development strongly augments heat stress induced gene expression in wild-type *C. elegans*[7]. These results suggested that the depletion of the COMPASS complex might increase the activity of the heat shock factor 1 (HSF-1), the master regulator of the eukaryotic proteostasis network[35,36]. We confirmed these results by monitoring the induction of the *hsp-16.2p::GFP* reporter before and after heat shock treatment (Fig. S2A, B), which showed significantly higher GFP expression in worms depleted for either *ash-2* or *set-2* compared to worms grown on control RNAi. This result was intriguing since presence of HSF-1 was not only reported to be crucial for lifespan regulation and protection against amyloid-mediated toxicity in *C. elegans*[22–24,37] but was also found to be most relevant for these processes when present during development[18,38]. These results made us now wonder whether the protective effect of knocking down members of the COMPASS complex

works directly through increasing HSF-1 activity. To test this idea, we depleted *hsf-1* in Q40::YFP animals, which were either maintained on control or *ash-2* RNAi bacteria and monitored their onset of paralysis. Consistent with previous results[18,24], knockdown of *hsf-1* sensitizes the Q40::YFP animals to amyloid toxicity and leads to significantly accelerated paralysis (Fig. 2A, black dashed trace) while depletion of *ash-2* delays the onset of paralysis (Fig. 2A, red solid trace). In combination, however, knockdown of *ash-2* failed to elicit any protective effect on *hsf-1* depleted worms (Fig. 2A, red dashed trace) despite similar knockdown efficiency in the strains (Fig. S2C). Worms grown on both *hsf-1* and *set-2* RNAi were even slightly more susceptible to Q40::YFP-mediated paralysis than *hsf-1*-deficient animals alone (Fig. S2D). Based on these results, we concluded that the mechanism by which depletion of H3K4me3 modifiers confers resistance to proteotoxicity requires the presence of functional HSF-1.

Effect of HSF-1 in H3K4me3 modifier-depleted worms is mediated by increased fat-7 levels

Neither analysis of the basal *hsp-16-2p::GFP* expression levels in non-amyloid expressing *C. elegans* (Fig. S2A, B) nor of HSP-16.2::mCherry fluorescence or mRNA levels of select HSF-1 controlled heat shock genes in Q40::YFP worms (Fig. S2E, F) revealed any significant differences between control and *ash-2* depleted worms, and only modest differences if any upon depletion of *set-2*. These results suggested that the observed increase in HSF-1 activity does not cause a constitutive activation of the heat shock response. This conclusion was fully consistent with global gene expression studies previously conducted in *ash-2* or *set-2* depleted non-amyloid expressing *C. elegans* strains[7,11,12] or performed in *ash-2* depleted Q40::YFP expressing worms for this study (Table S2). Neither dataset showed any global enrichment of stress-induced HSF-1 targets upon *ash-2* and/or *set-2* depletion. These results strongly suggested that the protective effect of HSF-1 is unlikely due to the constitutive upregulation of members of the proteostasis network but more likely due to changes in the expression levels of HSF-1 controlled non-heat shock genes. In fact, a recently conducted RNAseq analysis in *hsf-1*-depleted *C. elegans* revealed that HSF-1 controls

the expression of >1200 genes in a heat shock-*in*dependent manner, many of which specifically during *C. elegans* development[39]. Considering these findings, we therefore explored which HSF-1-controlled non-heat shock genes might be involved in the protective function of *ash-2* or *set-2*-depleted *C. elegans*. To our surprise, we noted stearoyl-CoA desaturase FAT-7, an enzyme that converts stearic acid into the mono-unsaturated fatty acid (MUFA) oleic acid[40,41] among the 15 most upregulated genes by HSF-1 in a heat shock *in*dependent manner [39]. Previous studies demonstrated that *ash-2* and *set-2* depleted *C. elegans* strains show increased levels of *fat-7* mRNA, which seemed responsible for the lifespan extension observed in H3K4me3 depleted worms[25]. Our results now suggested that increased activity of HSF-1 in *ash-2* or *set-2* depleted worms might constitute the missing link between a decrease in global H3K4me3 levels and an increase in *fat-7* mRNA levels. To test this idea, we determined *fat-7* mRNA expression levels in *ash-2* or *set-2* depleted Q40::YFP *C. elegans* using RT-PCR (Fig. 2B) and monitored GFP fluorescence in an *ash-2* or *set-2* depleted *fat-7p::fat-7::GFP* reporter strain (Fig. 2C-D). Both types of experiments not only confirmed the substantial increase in *fat-7* expression upon depletion of members of the COMPASS complex but demonstrated that the *fat-7* expression levels are tightly controlled by HSF-1. Knockdown of *hsf-1* by RNAi significantly decreased the *fat-7* expression levels in L4440 control, *ash-2* and *set-2* RNAi strains, essentially eliminating any increase in *fat-7* levels elicited by either *ash-2* or *set-2* depletion (Fig. 2B-D). These results strongly suggested that the increase in FAT-7 observed upon *ash-2* or *set-2* depletion is indeed the result of an increase in heat shock-independent HSF-1 activity. To test whether this increase in the levels of FAT-7 contributes to the protection of H3K4me3-depleted worms against amyloid toxicity, we maintained Q40::YFP expressing worms on either control, *ash-2* or *set-2* RNAi in the absence or presence of *fat-7* RNAi, and examined their paralysis. Indeed, we found that the knockdown of *fat-7* significantly accelerates paralysis in Q40::YFP worms and depletion of *ash-2* or *set-2* no longer conferred any protection (Fig. 2E). Based on these results, we concluded that

the protective effect elicited by the depletion of H3K4me3 modifiers involves the upregulation of HSF-1 activity, which leads to a substantial increase in protective FAT-7 levels.

Early-in-life upregulation of fat-7 protects against proteotoxicity later in life

Earlier studies revealed that whereas depletion of *hsf-1* during the entire lifespan of *C. elegans* (*i.e.,* development and adulthood) causes significantly shortened lifespan and accelerated paralysis, depletion of *hsf-1* during adulthood alone had only mild effects[18,38]. We now reasoned that if our model was indeed correct and HSF-1 mediated upregulation of FAT-7 responsible for our observed phenotypes, we should expect to find i) an increase in *fat-7* levels in worms transiently exposed to ROS during development, and ii) a primarily developmental requirement of *fat-7* expression for the protective effect later in life. To address the first prediction, we exposed *C. elegans* expressing the FAT-7::GFP reporter protein to the previously established 10-h bolus of paraquat at the L2 larval stage, and monitored FAT-7::GFP expression (Fig. 2F). To address the second aspect, we maintained Q40::YFP worms on *fat-7* RNAi either during their entire life or during adulthood only, and monitored their onset of paralysis (Fig. 2G). The results of both studies fully supported our model. We found that exposure of worms to early-in-life oxidative stress triggered a significant increase in FAT-7 levels in adult worms (Fig. 2F). Moreover, depletion of *fat-7* during adulthood alone had no major effects while depletion of *fat-7* during both development and adulthood significantly increased their sensitivity towards Q40-mediated proteotoxicity (Fig. 2G). While these results do not explain how FAT-7 expression in early life protects against proteotoxicity later in life, they do represent a further step towards finding the long-sought after mechanistic explanation for the temporal requirements of HSF-1 expression during *C. elegans* development[18,38].

Oleic acid protects against amyloid-induced proteotoxicity in an HSF-1-dependent manner

Recent studies revealed that exogenous addition of the FAT-7 product oleic acid to the growth media extends worm lifespan and protects against amyloid-induced proteotoxicity[25,42,43]. Indeed, comparison between the onset of paralysis in Q40::YFP worms grown on *ash-2* RNAi bacteria or on media supplemented with oleic acid revealed a striking resemblance, with both interventions causing a comparable delay in the onset of paralysis resemblance (Fig. 3A, *black dashed and red solid traces*). No further delay in paralysis was observed when we grew *ash-2* RNAi worms on media supplemented with oleic acid (Fig. 3A, *red trace*), suggesting that the depletion of *ash-2* leads to the production of optimally protective amounts of oleic acid. Consistent with this model, we also found that neutral lipid levels, as determined by Oil Red O staining, significantly increased upon *ash-2* depletion and reached levels comparable to control RNAi worms cultivated in the presence of oleic acid (Fig. 3B, compare grey and dark pink symbols). Yet, contrary to our model, we found that oleic acid supplementation did not rescue the premature paralysis phenotype of the *hsf-1* deficient animals (Fig. 3A, *purple traces*). The results were entirely unexpected given that oleic acid supplementation should be sufficient to compensate for the decreased *fat-7* expression in *hsf-1* depleted worms. They could also not be explained by issues in the uptake of oleic acid; in fact, we noted that *hsf-1* depleted worms have an even higher Oil Red O signal compared to wild-type or *ash-2* depleted worms when grown on oleic acid (Fig. 3B). Furthermore, we observed that, when cultured on oleic acid supplemented plates, *hsf-1* depleted Q40::YFP worms no longer display the developmental growth defect that we found associated with decreased *hsf-1* levels (Fig. 3C, D). These results indicated that *hsf-1* depleted worms are able to take up and utilize supplemented oleic acid to overcome their developmental defects. Yet, they seem unable to utilize the fatty acid in a way that provides protection against proteotoxicity later in life. We excluded the possibility that oleic acid exerts its beneficial effects through activating the heat shock response (Fig. S3A-D), and determined that the ability of free fatty acids to protect against proteotoxicity is selective towards oleic acid, as supplementation of the growth media with linoleic

acid, the first derivative of oleic acid, for instance, did not protect worms against Q40::YFP toxicity (Fig. S3E). These findings indicated that HSF-1 either directly or indirectly controls one or more additional steps downstream of oleic acid production, which are necessary to protect *C. elegans* against amyloid toxicity later in life.

HSF-1 mediated oleic acid utilization appears critically important to protect against amyloid toxicity

Our data strongly suggested that the protective effect of downregulating members of the COMPASS complex during development is caused by HSF-1-mediated changes in lipid composition and/or utilization. To assess how depletion of *ash-2* affects the lipid distribution of Q40::YFP expressing *C. elegans* and determine the role that HSF-1 plays in this process, we cultivated worms on either L4440 control, *ash-2*, *hsf-1,* or *ash-2* + *hsf-1* RNAi in the absence or presence of oleic acid, and conducted lipidomic analysis at day 1 of adulthood. We analyzed the distribution of over 700 different lipid species using non-targeted liquid chromatography mass spectrometry (LC-MS/MS) analysis (Figure 4; Table S3). As illustrated in the heatmap, we found that the most profound changes upon depletion of *ash-2* involved alterations in triacylglycerides (TGs), the main energy reservoirs in animals, with many TG species increasing in their relative abundance compared to worms grown on control RNAi (Fig. 4A). Unexpectedly, most of these changes were lost upon the additional depletion of *hsf-1*. In fact, knockdown of *hsf-1* caused a major general shift in the lipid landscape with lipids abundantly present in control or *ash-2* depleted Q40::YFP strains being substantially less abundant in worms grown on *hsf-1* RNAi and *vice versa* (Fig. 4A). Principal component analysis agreed with these conclusions, and showed that the significant differences in lipid composition between *ash-2* depleted and control RNAi worms are primarily mediated by HSF-1 (Fig. 4B); only 5 lipids were found to be significantly different in abundance when we compared the lipid composition of *ash-2* + *hsf-1* depleted Q40::YFP worms with that of *hsf-1* depleted worms whereas almost 18% of total lipids were different when we compared them with *ash-2* depleted worms (Fig. 4C). Closer analysis of the

compositional changes in TGs associated with the protective *ash-2* depletion revealed an enrichment for short and mono-unsaturated fatty acids (C<16) over longer and poly-unsaturated longer fatty acids in TGs (Fig. 4D, E; Fig. S4A). Depletion of *hsf-1*, on the other hand, had precisely the opposite effect; a pronounced increase in the ratio of polyunsaturated fatty acids over saturated and mono-unsaturated fatty acids stored in TGs, and the accumulation of very long chain fatty acids (Fig. 4D, E). These results were fully consistent with lipid composition changes in other long-lived mutants of *C. elegans*[44,45], providing further evidence for the emerging model that changes in TG composition might be a central unifying feature of mutations that lead to extended health and lifespan[46]. Yet our biggest surprise came when we realized that C18:1 species (*i.e.,* oleic acid, *cis*-vaccenic acid) did not accumulate upon *ash-2* depletion but were actually even lower than the C18:1 amounts measured in *hsf-1* depleted worms, which showed C18:1 levels comparable to wild-type or *ash-2* depleted worms grown on oleic acid supplemented plates for several days (Fig. 4E, last panel). These results were puzzling given that *fat-7* expression levels are increased upon *ash-2* depletion and hence should yield in higher C18:1 levels compared to *hsf-1* depleted worms, which show significantly decreased *fat-7* expression levels (Fig. 2B). Yet they fit to the idea that not the storage of oleic acid but its subsequent utilization make this fatty acid beneficial for the health and lifespan in *C. elegans*. Based on the finding that *hsf-1* depleted worms have significantly lower *fat-7* expression levels, we must also assume that much of the detected C18:1 species in *hsf-1* depleted worms is not oleic acid but *cis*-vaccenic acid (C18:1-Δ11), whose synthesis is catalyzed by the desaturase *fat-5*. Supplementing *hsf-1* depleted worms with additional oleic acid caused a further re-distribution of the TGs, leading to the further accumulation of very long-chain PUFAs at the expense of MUFAs (Fig. 4E). These results further supported our conclusion that *hsf-1* depleted worms lack the capacity to effectively utilize oleic acid, and explained why supplementation with oleic acid does not protect *hsf-1* depleted worms against proteotoxicity (Fig. 3A). To fully exclude that HSF-1's protective effects on amyloid proteotoxicity are mediated by changes in lipid utilization rather than

lipid storage, we used worms expressing the lipid droplet marker *dhs-3p::dhs-3::GFP*, and monitored their lipid droplet formation upon growth on control, *ash-2, hsf-1* and *ash-2 hsf-1* RNAi in the absence or presence of oleic acid. As previously shown[47], depletion of *hsf-1* leads to a decrease in DHS-3::GFP fluorescence signal, which is unaffected by oleic acid supplementation (Fig. 4F, Fig. S4C, D) and suggestive of defects in lipid droplet formation. However, depletion of *ash-2* as well as supplementing control RNAi worms with oleic acid also caused a significant reduction in DHS-3::GFP fluorescence signal, which was particularly noticeable in day 1 adult (Fig. 4F). By day 5 of adulthood, however, both control and *ash-2* RNAi strains had similar DHS-3::GFP signals, which were not only significantly higher compared to *hsf-1* depleted worms but also further increased upon oleic acid supplementation (Fig. S4C, D). These results ruled out a direct correlation between lipid droplet levels and proteotoxicity, and further supported the conclusion that increased lipid utilization in early adulthood might protect against proteotoxicity later in life.

HSF-1 controls the committed step of fatty acid oxidation

Given the observed differences in lipid composition and potential utilization in *ash-2* and *hsf-1*-depleted animals, we next assessed the changes in the expression of genes associated with lipid metabolic processes in Q40::YFP worms grown on control, *ash-2*, *hsf-1* or *ash-2* + *hsf-1* RNAi. Not surprisingly, we found many of the gene expression changes associated with the *ash-2* depletion to be reversed upon depletion of *hsf-1* (Fig. 5A). Metabolic pathway enrichment analysis further supported our lipidomics results and revealed an enrichment of genes involved in fatty acid biosynthesis and degradation pathways, particularly upon depletion of *hsf-1* (Fig. 5B, C; Fig. S5A). One of the genes most positively affected in *ash-2* versus *ash-2 hsf-1* depleted Q40::YFP worms encoded for acyl-CoA dehydrogenase 1 (ACDH-1) (Fig. 5D), the enzyme which catalyzes the committed step of mitochondrial fatty acid oxidation[48]. In fact, *acdh-1* had previously been shown to be one of the top genes whose expression is dependent upon HSF-1 in wild-type *C.*

elegans under non-stress conditions[39]. We further confirmed this result by RT-PCR and found that Q40::YFP animals deficient in *hsf-1* show an over 90% reduction in *acdh-1* mRNA (Fig. S5B). In addition to *acdh-1* expression, depletion of *hsf-1* alone (Fig. S5C) or in the background of *ash-2* depleted worms (Fig. 5D) also negatively affected the expression of several other proteins involved in mitochondrial β-oxidation, including *hacd-1* as well as *ech-7*, the enzyme catalyzing the second step in mitochondrial β-oxidation[40]. Based on these results and given that fatty acids like oleic acid are thought to be preferentially targeted toward the mitochondria for degradation[40], we now wondered whether the beneficial effects of *ash-2* depletion or oleic acid supplementation are caused by an HSF-1-mediated increase in β-oxidation, a lipid-metabolic process previously also associated with lifespan extension[49–52]. To test whether this is indeed the case, we maintained Q40::YFP worms on L4440, *ash-2, hsf-1,* or *ash-2* + *hsf-1* RNAi in the presence or absence of perhexiline (PHX). This compound disrupts fatty acyl transport into the mitochondria through the inhibition of the carnitine palmitoyl transporters, and has successfully been used to interrogate the effects of β-oxidation on lifespan in *C. elegans*[53]. Whereas PHX treatment alone showed little effect on the onset of paralysis in Q40::YFP worms grown on control RNAi, it completely abolished the protective effects triggered by *ash-2* depletion (Fig. 5E). No additional detrimental effects were observed when we treated *hsf-1* or *ash-2* + *hsf-1* depleted worms with PHX (Fig. 5E). These results provided first evidence that the transport of fatty acyls into mitochondria might be critical for the protective effects of *ash-2* depletion. Once transported into the mitochondria, fatty acids are broken down via β-oxidation to yield NADH, $FADH_2$, and acetyl-CoA for mitochondrial respiration. To determine whether there are any associated changes in mitochondrial respiration upon *ash-2* depletion, we measured the oxygen consumption rate (OCR) in Q40::YFP worms maintained on L4440, *ash-2*, *hsf-1*, or *ash-2* + *hsf-1* RNAi in the presence or absence of oleic acid using a Seahorse XFe96 analyzer (Fig. 5F). Intriguingly, the obtained OCR data effectively mirrored our earlier paralysis results (Fig. 3A). Whereas Q40::YFP worms maintained on either *ash-2* RNAi or control RNAi worms cultivated on oleic acid had

significantly higher OCRs compared to the respective controls, *hsf-1* depleted worms showed significantly decreased OCRs. This defect became particularly obvious when we compared the OCRs of *ash-2* + *hsf-1* depleted with *ash-2* depleted worms (Fig. 5F). Furthermore, supplementation of *hsf-1* depleted worms with oleic acid had either no or only very modest stimulatory effects on *hsf-1* depleted worms, suggesting that *hsf-1* depleted worms are unable to utilize supplemented oleic acid as energy source. Conducting the same experiments in the presence of perhexiline (PHX) further confirmed these conclusions (Fig. 5G), and showed that treatment with PHX significantly reduced the OCR of Q40::YFP worms grown on either control or *ash-2* RNAi yet failed to significantly affect the OCR of *hsf-1* depleted worms. These results not only demonstrated that HSF-1 plays a significant role in stimulating mitochondrial β-oxidation, but provided further proof for the model that disruption of H3K4me3 modifiers like *ash-2* protect organisms against proteotoxicity through a combination of oleic acid production and utilization early in life (Fig. 6).

Discussion

Uncovering the H3K4me3 – HSF-1 – Lipid Homeostasis – Proteotoxicity Axis

H3K4me3 modifiers of the COMPASS complex have been shown to play fundamentally important roles in the regulation of organismal lifespan and stress resistance in a variety of different organisms[7,11,25,54,55]. Yet, a particularly intriguing aspect came to light with the recent discovery that the transient oxidative inactivation of components of the COMPASS complex during *C. elegans* development, either elicited by natural variations in endogenous ROS levels or drug-induced, was sufficient to significantly extend lifespan[7]. These results added to a growing body of evidence that longevity effects can be achieved by appropriate early-in-life interventions[7–9,56]. We now show that transient exposure to ROS in early life not only extends lifespan but also significantly delays the onset of amyloid toxicity in *C. elegans* mutants expressing disease-related amyloids. These results provide further support for the newly emerging *Geroscience hypothesis*,

which states that interventions that extend organismal lifespan might be suitable to also delay the onset age-associated diseases[57]. However, they also re-emphasized the need to mechanistically explore how early-in-life events, such as those elicited by the oxidative downregulation of the COMPASS complex, work to protect against proteotoxicity and other age-related processes late in life. We now discovered that depletion of H3K4me3 modifiers triggers the functional upregulation of HSF-1 activity, the master regulator of the eukaryotic proteostasis network. Based on the prevailing idea that a decline in proteostasis contributes to aging and aging-associated diseases, HSF-1 has long been considered to serve as longevity factor through its central role in controlling the expression of chaperones and other folding factors[35]. Yet, some studies suggested some additional, proteostasis-independent effects of HSF-1 on organismal life- and healthspan. It has been shown, for instance in worms, that the activity of HSF-1 to extend lifespan and protect against amyloid toxicity either alone or in the context of other longevity paradigms, is most critical during the developmental phase while depletion of *hsf-1* during adulthood had only minor detrimental effects[18,38]. These results fit also to the finding that HSF-1 activity substantially decreases upon transition into the adulthood[58]. Yet, these results left the intriguing question open as to how HSF-1 can maintain protein homeostasis despite its natural decline in activity. Finally, RNAseq results indicated that HSF-1 controls the expression of more non-heat shock genes than heat shock genes particularly during development, suggesting additional roles of this highly conserved transcription factor beyond its involvement in cellular proteostasis[36,39]. We now demonstrate that by controlling the levels of desaturases (*e.g.,* FAT-7), lipases (*e.g.,* LIPL-2) and enzymes involved in fatty acid oxidation (*e.g.,* ACDH-1, ECH-7), HSF-1 greatly influences the lipid homeostasis in *C. elegans*, enhancing both the production of protective MUFAs, such as oleic acid, as well as their subsequent utilization through mitochondrial β-oxidation. Importantly, genetic epistasis experiments and inhibitor studies strongly suggest that this HSF-1 mediated combination of increased MUFA synthesis and utilization play a major role in combating proteotoxicity. Intriguingly, all three events, H3K4me3 depletion, HSF-1 upregulation, and

increased MUFA production appear to be critically important during development to protect against proteotoxicity later in life. Based on these findings, we now propose that HSF-1 mediated changes in lipid homeostasis and metabolism might constitute the mechanism by which early-in-life events are manifested and affect proteotoxicity and potentially other age-associated processes later in life (Fig. 6).

HSF-1 – Protecting against proteotoxicity through changes in lipid composition and utilization

Changes in lipid composition and metabolism are increasingly being associated with extended lifespan and healthspan in a variety of different organisms[25,42,43,59–61]. For instance, an increase in membrane-associated MUFAs over PUFAs has been shown to associate with longer lifespan, possibly due to the reduced peroxidation sensitivity of MUFAs and hence a mitigation of age-associated oxidative damage[62]. Similarly, in a variety of different longevity paradigms, including insulin signaling mutants, both synthesis, mobilization and subsequent utilization of neutral acids like oleic acid was found to be significantly increased[44]. Moreover, supplementation with oleic acid supplementation has been shown to be beneficial for extended lifespan and healthspan[25,42,43]. Our studies now demonstrated, however, that increasing the synthesis of or supplementing growth media with oleic acid are ineffective measures in protecting *C. elegans* against amyloid toxicity. In fact, HSF-1 depleted worms, which are unable to utilize oleic acid through mitochondrial β-oxidation, accumulate vast amounts of C18:1 species in addition to PUFAs and other longer-chain fatty acids, which potentially contribute to their premature paralysis and cell death phenotypes. Several recent studies also implicated increases in β-oxidation with lifespan extension[49,50,52,53,63], although the systematic knockdown of the nine genes involved in mitochondrial β-oxidation in worms gave much less clear results[51]. Knockdown of only one of these genes resulted in a shorter lifespan while knockdown of the others either did not affect lifespan or even extended lifespan. Conducting the same experiments in longer-lived germline mutants of *C. elegans*, however, revealed that knockdown of every single one of these genes

significantly shortened their lifespan. We made similar observations when perhexiline exposure, which reportedly blocks mitochondrial β-oxidation, did not affect paralysis in the control worms but abolished the protective effects in the long-lived *ash-2* depleted animals (Fig. 5E). These results suggest that the effects of alterations in β-oxidation to promote stress resistance or extend lifespan might be context-specific. Given that the previous studies did not directly measure β-oxidation through OCR analysis or other methods but used changes in the expression of genes involved in β-oxidation as proxy, further investigations are clearly needed to determine when in life and how increases in mitochondrial β-oxidation promote stress resistance and longevity.

HSF-1 depleted worms show signs of lipid starvation

Recent work from Watterson *et al.* demonstrated that depletion of *hsf-1* causes a significant decrease in lipid droplet formation, which was proposed to be triggered by the activation of the nuclear hormone receptor NHR-49[47], a transcription factor known to up-regulate a number of genes involved in β-oxidation[51]. Yet, our oxygen consumption rate measurements did not provide any evidence that *hsf-1* depleted worms show any increase in mitochondrial fatty acid oxidation (Fig. 5F). In contrast, OCRs in *hsf-1* depleted worms were extremely reduced, non-responsive to oleic acid supplementation and unaffected by perhexiline, an established inhibitor of fatty acid oxidation. These results strongly suggested that *hsf-1* depleted worms lack the capacity to utilize oleic acid and potentially other fatty acids as energy source, resulting in a starvation-like state[47]. Indeed, the observed transcriptional upregulation of many lipases in *hsf-1*-depleted animals (Fig. S5C) may be reflective of cellular attempts to access lipid stores and increase lipid mobilization under these conditions. We now argue that it is this inability of *hsf-1* depleted worms to appropriately utilize TGs that leads to the activation of *nhr-49*, which further depletes lipid stores, and causes a major redistribution of the cellular lipid composition. It is also of note that while the number of DHS-3-positive lipid droplets observed in *hsf-1* depleted worms does not significantly increase upon supplementation with oleic acid, the Oil red O signal, which stains for neutral lipids

in fixed worms, was significantly higher in *hsf-1* depleted strains compared to the control strains upon oleic acid supplementation. These results confirm that *hsf-1* depleted worms are unable to either utilize or appropriately store the lipids in DHS-3-positive compartments. Subsequent modification of these incorrectly stored lipids might contribute to the massively altered lipid profile found in *hsf-1* depleted worms.

Upregulation of HSF-1 Activity through COMPASS complex depletion

Our studies revealed a previously unknown connection between decreased levels of H3K4me3 modifiers and increased activity of HSF-1. These results were consistent with previous reports, which showed that depleting members of the COMPASS complex augments the heat shock response in both *C. elegans* and cell culture models[7] and causes increased steady state expression of a large number of HSF-1 controlled non-heat shock genes in both wild-type and Q40::YFP expressing worms (this study) without affecting HSF-1 mRNA levels[7]. These results however also raised the obvious question as to how depletion of H3K4me3, a mark considered to be activating and reflective of transcriptional memory[64], leads to increased transcriptional activity of HSF-1. Previous work showed that HSF-1 function in worms is regulated by the activity of the H3K27me3 demethylase JMJD-3.1, which removes the repressive H3K27me3 mark from heat shock promoter regions, thus enhancing HSF-1 activity during development[58]. Upon transition into adulthood, however, a germline-dependent downregulation of *jmjd-3.1* causes the accumulation of the repressive mark on HSF-1 promoters, and hence explains the previously observed decrease in HSF-1 activity in adult worms[58]. It now remains to be seen whether the oxidative downregulation of H3K4me3 levels either directly or indirectly affects other marks, such as H3K27me3 on HSF-1-controlled heat shock and non-heat shock promoters. Intriguingly, the contribution of *ash-2* in COMPASS complex activity (*i.e.,* tri- and demethylation of H3K4) has recently been shown to also vary depending on the tissue and developmental stage of the worms[65]. Given the phenotypical differences that we and others observe between the *set-2* and

a*sh-2* depletion strains, with the latter showing reproducibly more protective phenotypes (this study) and longer lifespan[11], it is also possible that changes in H3K4me2 levels rather than H3K4me3 levels affect the promoter occupancy and transcriptional activity of HSF-1. Finally, it is conceivable that depletion of members of the COMPASS complex affect one or more posttranslational modifications on HSF-1, which are known to regulate HSF-1 stability, activity and specificity[66]. Future studies are needed to mechanistically dissect this previously unknown link between early-in-life histone modifications and the activity of one of the best known longevity factors in biology.

Methods

***C. elegans* strains, maintenance, and synchronization.** The following strains of *C. elegans* were used in this study: CL4176 (*dvIs27 [myo-3p::Aβ (1-42)::let-851 3'UTR) + rol-6(su1006)]);* CL2006 (*dvIs2 [pCL12(unc-54/human Aβ peptide 1-42 minigene) + rol-6(su1006)]);* AM141 *(rmIs133 [unc-54p::Q40::YFP]);* UJ002 *(dvIs2; set-2(ok952));* UJ001 *(rmIs12; set-2(ok952))*; CL2070 (*dvIs70 [hsp-16.2p::GFP + rol-6(su1006)]);* DMS303 *(nIs590 [fat-7p::fat-7::GFP + lin15(+)]);* PHX4983 *(syb4983 [hsp-16.2p::hsp-16.2::mCherry]);* UJ003 *(rmIs13*; *syb4983);* LIU1 *(ldrIs1 [dhs-3p::dhs-3::GFP + unc-76(+)]);* GRU102 *(gnaIs2 [myo-2p::YFP + unc-119p::Abeta1-42]).* Transgenic PHX4983 animals were generated by SunyBiotech (Fuzhou, China) using CRISPR/Cas9-mediated knock-in of *hsp-16.2::mCherry* at the endogenous locus. Worms were maintained per standard protocols on NGM plates containing streptomycin and nystatin seeded with streptomycin-resistant *Escherichia coli* OP50[67]. Strains expressing Aβ were maintained at 15°C, and all other strains at 20°C. Synchronized populations of worms were obtained by transferring gravid adults to new plates, allowing them to lay eggs for 2-3 h, then removing the adults.

Paralysis and lifespan assays. CL2006 and Q40::YFP animals were synchronized by timed egg lay, transferred to fresh plates when they reached day 1 of adulthood (defined as the first day that eggs appear on the plates, *t*=0 on graphs) and incubated at 20°C. Animals were moved to fresh plates as necessary to avoid contamination with their progeny. Paralysis assays in CL4176 animals were conducted using the temperature shifting regimen previously described[26], with slight modifications. Briefly, animals were synchronized by timed egg lay for 2 h and maintained at 15°C. 50 h after the egg lay, animals were shifted to 25°C. Paralysis was assessed beginning 32 h after temperature upshift by gentle prodding with a platinum worm pick. Animals that failed to propagate a full-body wave in response to stimulation were counted as paralyzed. Lifespan assessment in GRU102 animals was conducted at 20°C, with animals failing to respond to gentle prodding with

a platinum worm pick considered dead. Animals with vulval protrusions or internally-hatched embryos were censored. Data from paralysis assays were plotted with GraphPad Prism as survival curves and analyzed for statistical significance with the log-rank (Mantel-Cox) test. Statistics for all paralysis and lifespan experiments can be found in Table S1.

RNAi in *C. elegans*. RNAi was achieved through feeding worms *E. coli* HT115 (DE3) strains expressing dsRNA to genes of interest from the Ahringer RNAi library (a kind gift from Gyorgyi Csankovszki). Bacteria were seeded onto NGM plates containing ampicillin (50 µg/ml), tetracyclin (12.5 µg/ml), and IPTG (1 mM) at an OD_{600} of 0.8-1.0. Bacterial lawns were allowed to form for at least 48 h prior to worm placement. In the instances where multiple genes were targeted by RNAi, equal mixtures of the respective HT115 RNAi clones were seeded on plates. HT115 bacteria containing the empty L4440 vector used for dsRNA expression were used as a control. In all experiments using *ash-2* or *set-2* RNAi, worms were maintained on RNAi plates for one generation prior to the experimental population, as this has been found to increase the RNAi effect of *ash-2* or *set-2* knockdown. All experiments using other RNAi clones were conducted by hatching synchronized populations of eggs on RNAi plates, and conducting experiments in that population.

Western blotting. For western blotting of *C. elegans*, 150-200 adult worms were collected in 40 µl M9 buffer, to which 10 µl of 5X Laemmli loading buffer was added. Samples were boiled for 5 min and vortexed thoroughly until worms had completely solubilized. Electrophoresis, transfer, and blocking were conducted per standard protocols[7]. Primary and secondary antibodies were diluted in 1% w/v milk/tris-buffered saline, 0.1% Tween-20 and incubated at 4°C overnight, or at room temperature for 45 min, respectively. Bands were visualized using enhanced chemiluminescence (SuperSignal West Pico PLUS, ThermoFisher Scientific, 34580). The following primary and secondary antibodies were used in this study: anti-H3 (Abcam, ab1791; 1:2000); anti-H3K4me3 (Abcam, ab8580; 1:1000); anti-GFP (Novus Biologicals, NB600-303,

1:2000); anti-amyloid-β 1-16 (clone 6E10, BioLegend, 803001, 1:1000); anti-rabbit-horseradish peroxidase (ThermoFisher Scientific, 31460); anti-mouse-horseradish peroxidase (ThermoFisher Scientific, 31430).

Paraquat and MM-401 treatment. Paraquat (PQ; methyl viologen hydrate, ACROS Organics) or MM-401 (a kind gift from Yali Dou) was added to NGM plates at the indicated concentrations, allowed to solidify, and seeded with OP50. CL4176 animals maintained at 15°C were transferred to PQ-containing plates during the L2 stage (38 h post-egg lay) for 10 h, then moved back to NGM plates without PQ prior to temperature upshift to 25°C to stimulate Aβ production[26].

RNA isolation, cDNA synthesis, and qPCR. RNA isolation from *C. elegans* was performed per standard protocols with slight modifications[68]. Briefly, 20-25 adult animals were picked into a 5 µl drop of lysis buffer (5 mM Tris, pH 8.0, 0.5% v/v Triton X-100, 0.5% v/v Tween 20, 0.25 mM EDTA) containing 1 mg/ml proteinase K (New England BioLabs) in the lid of a PCR tube. Animals were centrifuged to the tube bottom, subjected to three rounds of freeze/thaw cycles with a dry ice/ethanol bath, and lysed in a thermocycler (65°C for 10 min, 85°C for 1 min). cDNA synthesis was performed using the iScript cDNA Synthesis Kit (Bio-Rad), and qPCR performed using Radiant Green Lo-ROX qPCR Kit (Alkali Scientific) per manufacturer's instructions. Reactions were performed in technical triplicate using *pmp-3* as a housekeeping gene, and relative gene expression was determined using the $2^{(-\Delta\Delta C_t)}$ method[69]. The following primers were used: *fat-7* (for) 5'-GCGCTGCTCACTATTTTGGT-3' and *fat-7* (rev) 5'-GTGGGAATGTGTGGTGGAAA-3'; *pmp-3* (for) 5'-TTTGTGTCAATTGGTCATCG-3' and *pmp-3* (rev) 5'-CTGTGTCAATGTC GTGAAGG-3'; *hsp-16.11* (for) 5'-TGGCTCAGATGGAACTGCAA-3' and *hsp-16.11* (rev) 5'-TGG CTTGAACTGCGAGACAT-3'; *hsp-16.2* (for) 5′-CTGTGAGACGTTGAGATTGATG-3′ and *hsp-16.2* (rev) 5′-CTTTACCACTATTTCCGTCCAG-3′; *hsp-16.48* (for) 5'-GCTCATGCTCCGTTCT CCAT-3' and *hsp-16.48* (rev) 5'-GAGTTGTGATCAGCATTTCTCCA-3'; *acdh-1* (for) 5'-CGAA ATGCAGATCCTAGCC-3' and *acdh-1* (rev) 5'-GTTTGTCTTCCTCCTTATCTACAG-3'; *ash-2* (for)

5’-CGCCTATTACCCGTCGATT-3’ and *ash-2* (rev) 5’-GTTTGTTCGTGTTGCTGCTC-3’; *hsf-1* (for) 5’-CTGGAGCAGCACGTCGTTAT-3’ and *hsf-1* (rev) 5’-CCGGATTTGTTCAAGGTCTCC-3’.

Fluorescence microscopy of *C. elegans*. Aggregation of Q40::YFP was visualized by mounting AM141 *C. elegans* on a 2% agarose pad placed on a microscope slide immobilized with 10 µl of levamisole (25 mM, MP Biomedicals LLC, Irvine, CA). Fluorescent reporter strains (*hsp-16.2p::GFP, fat-7p::fat-7::GFP, dhs-3p::dhs-3::GFP)* were imaged by picking worms into a small drop of levamisole on an unseeded NGM plate. Imaging was conducted immediately after levamisole drying on a Shimadzu Olympus or ECHO Revolution microscope using a 4X objective using with MetaMorph software. Quantification of Q40::YFP foci was performed in ImageJ (NIH) by manual counting in images with defined thresholds that were kept uniform across all conditions. Quantification of GFP fluorescence in fluorescent reporter strains *(fat-7p::fat-7::GFP, hsp-16.2p::GFP, dhs-3p::dhs-3::GFP)* was performed in ImageJ by measuring mean fluorescence intensity per animal. Assessment of HSP-16.2::mCherry levels in Q40::YFP; *hsp-16.2p::hsp-16.2::mCherry* animals was conducted on levamisole-immobilized animals on microscope slides containing 2% agarose pads. Animals were then imaged with a 20X objective on a Leica THUNDER imager using an excitation/emission of 475/535 nm for YFP and 575/590 nm for mCherry. All images within an experiment were acquired with uniform acquisition settings. Quantification of HSP-16.2::mCherry was performed in ImageJ by quantifying mean fluorescence intensity in the heads of animals.

Lipidomics. Total lipid extracts from C. elegans pellets were prepared using a modified MTBE lipid extraction protocol[70]. Briefly, 400 µL of cold methanol and 10 µL of internal standard mixture (EquiSPLASH lipidomix) were added to each sample followed by incubation at 4°C, 650 RPM shaking for 15 minutes. Next, 500 µL of cold MTBE was added followed by incubation at 4°C for 1 hour with 650 RPM shaking. 500 µL of cold water was added slowly and resulting extract was maintained 4°C, 650 rpm shaking for 15 minutes. Phase separation was completed by

centrifugation at 8,000 RPM for 8 min at 4 °C. The upper, organic phase was removed and set aside on ice. The bottom, aqueous phase was re-extracted with 200 µL of MTBE followed by 15 minutes of incubation at 4°C with 650 RPM shaking. Phase separation was completed by centrifugation at 8,000 RPM for 8 min at 4 °C. The upper, organic phase was removed and combined with previous organic extract. The organic extract was dried under a steady stream of nitrogen at 30 °C. The recovered lipids were reconstituted in 200 µL of chloroform:methanol (1:1, v/v) containing 200 µM of butylated hydroxytoluene. Prior to analysis samples were further diluted 10 fold with acetonitrile:isopropanol:water (1:2:1, v/v/v). The lower aqueous phase was used to determine the protein content via a BCA kit (bicinchoninic acid assay, Thermo Fisher Scientific, Rockford, USA).

Lipid Analysis. Total lipid extracts were analyzed by liquid chromatography coupled to high resolution tandem mass spectrometry (LC-MS/MS). The LC-MS/MS analyses were performed on an Agilent 1290 Infinity LC coupled to an Agilent 6560 Quadrupole Time-of-Flight (Q-TOF) mass spectrometer. The separation was achieved using an C18 CSH (1.7 µm; 2.1 x 100 mm) column (Waters, Milford, MA). Mobile phase A was 10 mM ammonium formate with 0.1% formic acid in water/acetonitrile (40:60, v/v) and mobile phase B was 10 mM ammonium formate with 0.1% formic acid in acetonitrile/isopropanol (10:90, v/v). The gradient was ramped from 40 % to 43 % B in 1 min, ramped to 50 % in 0.1 min, ramped to 54 % B in 4.9 minutes, ramped to 70 % in 0.1 min, and ramped to 99 % B in 2.9 min. The gradient was returned to initial conditions in 0.5 min and held for 1.6 min for column equilibration. The flow rate was 0.4 mL/min. The column was maintained at 55 °C and the auto-sampler was kept at 5 °C. A 2 µL injection was used for all samples. Mass spectrometry analysis was separated into two workflows: 1.) lipid identification of a pooled sample using an iterative MS/MS acquisition and 2.) lipid semi-quantitation of all samples using high-resolution, accurate mass MS^1 acquisition. The MS parameters for the iterative workflow were as follows: extended dynamic range, 2 GHz; gas temperature, 200°C; gas flow, 10

L/min; nebulizer, 50 psi; sheath gas temperature, 300°C; sheath gas flow, 12 L/min; VCap, 3.5kV (+), 3.0kV (–); nozzle voltage, 250V; reference mass *m/z* 121.0509, *m/z* 1221.9906 (+), *m/z* 119.0363, *m/z* 980.0164 (–); MS and MS/MS Range m/z 100–1700; acquisition rate, 3 spectra/s; isolation, narrow (~ 1.3 m/z); collision energy 20 eV (+), 25 eV (–); max precursors/cycle, 3; precursor abundance-based scan speed, 25,000 counts/spectrum; ms/ms threshold, 5,000 counts and 0.001%; active exclusion enabled yes; purity, stringency 70 %, cut off 0 %; isotope model, common organic molecules; static exclusion ranges, *m/z* 40 to 151 (+,–). The MS parameters for the MS^1 workflow were the same for source and reference mass parameters and differed only for acquisition.

LC-MS/MS data from the iterative MS/MS workflow was analyzed for lipid identification via Agilent's Lipid Annotator (v 1.0). The default settings for feature finding and identification parameters were used. Positive and negative ion mode adducts included $[M+H]^+$, $[M+Na]^+$, $[M+NH_4]^+$, $[M-H]^-$, and $[M+CH_3CO_2]^-$, respectively. The results of the Lipid Annotator were saved as a PCDL file. The LC-MS data from the MS^1 workflow were processed using Agilent's MassHunter Profinder (v 10.0). Batch targeted feature extraction using default parameters and the PCDL file created from Lipid Annotator were used for feature extraction. The processed data generated from Profinder which included peak area and lipid identification was exported into MetaboAnalyst 4.0[71] for multivariate analysis. Univariate analysis was done using Prism 6 (GraphPad, La Jolla, CA).

RNA extraction, sequencing, and pathway enrichment analysis. Day 1 adult *C. elegans* were collected from NGM plates by washing with M9. Animals were pelleted by centrifugation (1000 x g, 1.5 min), supernatant aspirated, and 10 mL of fresh M9 was added. This wash step was performed a total of 3 times. After washing, supernatant was aspirated away, leaving as little M9 as possible. A glass pipet was used to collect the pelleted worms, and immediately dropped into liquid nitrogen to form frozen pellets. Frozen pellets were homogenized in 250 µL TRIzol with 100

µL zirconia beads, using a bead mill homogenizer (Omni International, Inc). RNA was extracted using chloroform and concentrated using an Rneasy column (QIAGEN), following manufacturer's instructions. Dnase I digestion (Thermo Fisher Scientific) was then performed on eluted RNA per manufacturer's instructions, and samples stored at -80°C until further processing. RNA sequencing was conducted by LC Sciences (Houston, TX), where RNA integrity was first assessed using an Agilent Technologies 2100 Bioanalyzer. Poly(A) RNA sequencing libraries were generated using the TruSeq Stranded mRNA protocol (Illumina, Inc, San Diego CA). Oligo-(dT) magnetic beads were utilized to isolate mRNAs containing poly(A) tails, with two rounds of purification. Poly(A) RNA was then fragmented using divalent cation buffer in elevated temperature.. Paired-end sequencing was performed on the NovaSeq 6000 sequencing system (Illumina, Inc). Cleaning of the reads was performed using Cutadapt [72] and in-house perl scripts (LC Sciences), and sequence quality was assessed using FastQC (http://www.bioinformatics.babraham.ac.uk/projects/fastqc/). Reads were mapped to the *C. elegans* genome using HISAT2 [73], and mapped reads assembled into transcripts using StringTie [74]. Transcriptomes were compiled using perl scripts and gffcompare, and StringTie and ballgown (http://www.bioconductor.org/packages/release/bioc/html/ballgown.html) were used to determine mRNA expression levels by calculating FPKM. Differential mRNA expression analysis was performed using DESeq2[75] between two different groups and by R package edgeR[76] between two samples, with mRNAs with a false discovery rate (FDR) < 0.05 and absolute fold change ≥ 2 being considered as differentially expressed. Differentially expressed gene sets identified in RNA sequencing analysis were assessed for enrichment in metabolic pathways using the WormFlux Pathway Enrichment Analysis tool[77].

Fatty acid supplementation and Oil Red O (ORO) staining. Supplementation of NGM plates with oleic acid or linoleic acid was performed as previously described[25] with slight modifications. In brief, 0.01 % v/v NP-40 was added in all plates prior to autoclaving to aid in even distribution

of the fatty acids. Oleic acid sodium salt (Sigma, O7501) or linoleic acid sodium salt (Sigma, L8134) was added to molten NGM to a final concentration of 0.8 mM. Staining of *C. elegans* lipids was conducted using oil red O (ORO) as previously described[78]. ORO-stained worms were imaged on a stereoscope equipped with a SC50 color camera (Olympus). Lipid accumulation in whole animals was quantified in ImageJ by converting color images to grayscale, inverting images, and quantifying mean intensity in outlined worms.

Perhexiline treatment. Perhexiline (Cayman Chemicals, Ann Arbor, MI) was administered to *C. elegans* as previously described[53]. Immediately prior to animals being placed on plates, a 100 mM perhexiline stock solution was diluted to 2.5 mM perhexiline solution with ddH_2O, and 100 µL was pipetted onto the bacterial lawn of seeded NGM plates. For control plates without perhexiline, 100 µL of ddH_2O was added. Plates were allowed to dry, and after drying, animals were placed onto the plates. Perhexiline was administered from egg, and new plates prepared as needed when worm transfer was necessary.

Assessment of oxygen consumption rates in *C. elegans*. Oxygen consumption rates (OCRs) were measured using a Seahorse Xfe96 Analyzer (Agilent Technologies) as previously described[79]. Briefly, day 1 adult Q40::YFP worms (96 h post egg) were collected by washing from plates in M9 buffer, and worms added to the wells of an Xfe96 well plate in 200 µl volume. The baseline oxygen consumption rate was assessed five times per condition using a program of 2 min mixing, 0.5 min waiting, and 2 min measuring. Measurements were performed at room temperature (~27°C to 30°C with heat from the instrument). Five technical replicates were used per experimental condition, with wells containing an average of 15 worms/well. Wells containing fewer than five worms were excluded from analysis. Statistically significant changes in OCR were determined by one-way ANOVA with Fisher's LSD test.

Acknowledgments

We thank the Csankovszki lab for providing us with RNAi bacteria, and the members of the Jakob and Bardwell lab for many helpful discussions. This work was supported by the National Institute of Health grant R35 GM122506 and the National Institute of Aging grant R21 AG078540 to U.J, a Bright Focus ADR Fellowship (A2019250F) to B.J.O., and a University of Michigan T32-AG000114 Career Training in the Biology of Aging Training Grant to B.J.O. and D. B. In addition, the work was supported by the University of Maryland School of Pharmacy Faculty Start-up funds, the University of Maryland School of Pharmacy Mass Spectrometry Center (SOP1841-IQB2014) and an NIH R21NS117867 award to J.W.J.

Author Contributions

B.J.O., conceptualization, investigation, formal analysis, methodology, supervision, writing – original draft and writing – review & editing; J.B., conceptualization, investigation; S.L.Z., investigation; T.K., investigation; Y.J., investigation, formal analysis; E.J., investigation; C.L., investigation; C.M., investigation; D.B., conceptualization; J.W.J., methodology, formal analysis, resources, project administration, supervision, funding acquisition; U.J., conceptualization, project administration, supervision, funding acquisition, writing – original draft and writing - review & editing.

Declaration of Interests

The authors declare no competing interests.

Data and Code Availability

- Mass spectrometry data used for lipidomic analysis are deposited in Mendeley Data http://dx.doi.org/10.17623/hw2k9gkhnb.1.
- RNAseq data: https://www.ncbi.nlm.nih.gov/geo/query/acc.cgi?acc=GSE227652 Reviewer Token: uzyjsukshbalxqh

References

1. Kenyon, C. J. The genetics of ageing. *Nat. 2010 4647288* **464**, 504–512 (2010).

2. Kirkwood, T. B. L. & Finch, C. E. Ageing: The old worm turns more slowly. *Nature* **419**, 794–795 (2002).

3. Klass, M. R. Aging in the nematode Caenorhabditis elegans: major biological and environmental factors influencing life span. *Mech. Ageing Dev.* **6**, 413–429 (1977).

4. Herndon, L. A. *et al.* Stochastic and genetic factors influence tissue-specific decline in ageing C. elegans. *Nat. 2002 4196909* **419**, 808–814 (2002).

5. Johnson, T. E. Increased life-span of age-1 mutants in Caenorhabditis elegans and lower gompertz rate of aging. *Science (80-.).* **249**, 908–912 (1990).

6. Knoefler, D. *et al.* Quantitative in vivo redox sensors uncover oxidative stress as an early event in life. *Mol Cell* **47**, 767–776 (2012).

7. Bazopoulou, D. *et al.* Developmental ROS individualizes organismal stress resistance and lifespan. *Nature* **576**, (2019).

8. Shindyapina, A. V. *et al.* Rapamycin treatment during development extends life span and health span of male mice and Daphnia magna. *Sci. Adv.* **8**, eabo5482 (2022).

9. Sun, L., Sadighi Akha, A. A., Miller, R. A. & Harper, J. M. Life-span extension in mice by preweaning food restriction and by methionine restriction in middle age. *J Gerontol A Biol Sci Med Sci* **64**, 711–722 (2009).

10. Shilatifard, A. The COMPASS family of histone H3K4 methylases: mechanisms of regulation in development and disease pathogenesis. *Annu Rev Biochem* **81**, 65–95 (2012).

11. Greer, E. L. *et al.* Members of the H3K4 trimethylation complex regulate lifespan in a germline-dependent manner in C. elegans. *Nature* **466**, 383–387 (2010).

12. Pu, M., Wang, M., Wang, W., Velayudhan, S. S. & Lee, S. S. Unique patterns of trimethylation of histone H3 lysine 4 are prone to changes during aging in Caenorhabditis elegans somatic cells. *PLoS Genet* **14**, e1007466 (2018).

13. Hou, Y. *et al.* Ageing as a risk factor for neurodegenerative disease. *Nat. Rev. Neurol. 2019 1510* **15**, 565–581 (2019).

14. Jimenez-Sanchez, M., Licitra, F., Underwood, B. R. & Rubinsztein, D. C. Huntington's Disease: Mechanisms of Pathogenesis and Therapeutic Strategies. *Cold Spring Harb. Perspect. Med.* **7**, a024240 (2017).

15. Querfurth, H. W. & LaFerla, F. M. Alzheimer's Disease. *http://dx.doi.org/10.1056/NEJMra0909142* **362**, 329–344 (2010).

16. Hipp, M. S., Kasturi, P. & Hartl, F. U. *The proteostasis network and its decline in ageing*. vol. 20 421–435 (Nature Publishing Group, 2019).

17. Cohen, E. *et al.* Reduced IGF-1 Signaling Delays Age-Associated Proteotoxicity in Mice. *Cell* **139**, 1157–1169 (2009).

18. Cohen, E., Bieschke, J., Perciavalle, R. M., Kelly, J. W. & Dillin, A. Opposing activities protect against age-onset proteotoxicity. *Science (80-.).* **313**, 1604–1610 (2006).

19. Cao, Q. *et al.* Targeting histone K4 trimethylation for treatment of cognitive and synaptic deficits in mouse models of Alzheimer's disease. *Sci. Adv.* **6**, (2020).

20. Kaeberlein, M. & Galvan, V. Rapamycin and Alzheimer's disease: Time for a clinical trial? *Sci. Transl. Med.* **11**, 4289 (2019).

21. Steinkraus, K. A. *et al.* Dietary restriction suppresses proteotoxicity and enhances longevity by an hsf-1-dependent mechanism in Caenorhabditis elegans. *Aging Cell* **7**, 394–404 (2008).

22. Nollen, E. A. A. *et al.* Genome-wide RNA interference screen identifies previously undescribed regulators of polyglutamine aggregation. *Proc. Natl. Acad. Sci. U. S. A.* **101**, 6403–6408 (2004).

23. Katsuno, M. *et al.* Pharmacological induction of heat-shock proteins alleviates polyglutamine-mediated motor neuron disease. *Proc. Natl. Acad. Sci. U. S. A.* **102**, 16801–16806 (2005).

24. Hsu, A. L., Murphy, C. T. & Kenyon, C. Regulation of aging and age-related disease by DAF-16 and heat-shock factor. *Science (80-.).* **300**, 1142–1145 (2003).

25. Han, S. *et al.* Mono-unsaturated fatty acids link H3K4me3 modifiers to C. elegans lifespan. *Nature* (2017) doi:10.1038/nature21686.

26. Dostal, V. & Link, C. D. Assaying β-amyloid Toxicity using a Transgenic C. elegans Model. *JoVE (Journal Vis. Exp.* e2252 (2010) doi:10.3791/2252.

27. Cao, F. *et al.* Targeting MLL1 H3K4 Methyltransferase Activity in Mixed-Lineage Leukemia. *Mol. Cell* (2014) doi:10.1016/j.molcel.2013.12.001.

28. Link, C. D. Expression of human β-amyloid peptide in transgenic Caenorhabditis elegans. *Proc. Natl. Acad. Sci. U. S. A.* **92**, 9368–9372 (1995).

29. Link, C. D. C. elegans models of age-associated neurodegenerative diseases: Lessons from transgenic worm models of Alzheimer's disease. *Exp. Gerontol.* **41**, 1007–1013 (2006).

30. Teo, E. *et al.* Metabolic stress is a primary pathogenic event in transgenic Caenorhabditis

elegans expressing pan-neuronal human amyloid beta. *Elife* **8**, (2019).

31. Morley, J. F., Brignull, H. R., Weyers, J. J. & Morimoto, R. I. The threshold for polyglutamine-expansion protein aggregation and cellular toxicity is dynamic and influenced by aging in Caenorhabditis elegans. *Proc. Natl. Acad. Sci. U. S. A.* **99**, 10417–10422 (2002).

32. Walther, D. M. *et al.* Widespread Proteome Remodeling and Aggregation in Aging C. elegans. *Cell* **161**, 919–932 (2015).

33. Rahman, M. M. & Lendel, C. Extracellular protein components of amyloid plaques and their roles in Alzheimer's disease pathology. *Mol. Neurodegener. 2021 161* **16**, 1–30 (2021).

34. Xiong, F., Ge, W. & Ma, C. Quantitative proteomics reveals distinct composition of amyloid plaques in Alzheimer's disease. *Alzheimer's Dement.* **15**, 429–440 (2019).

35. Åkerfelt, M., Morimoto, R. I. & Sistonen, L. Heat shock factors: Integrators of cell stress, development and lifespan. *Nature Reviews Molecular Cell Biology* at https://doi.org/10.1038/nrm2938 (2010).

36. Li, J., Labbadia, J. & Morimoto, R. I. Rethinking HSF1 in Stress, Development, and Organismal Health. *Trends Cell Biol.* **27**, 895–905 (2017).

37. Morley, J. F. & Morimoto, R. I. Regulation of Longevity in Caenorhabditis elegans by Heat Shock Factor and Molecular Chaperones. *Mol. Biol. Cell* **15**, 657–664 (2004).

38. Volovik, Y. *et al.* Temporal requirements of heat shock factor-1 for longevity assurance. *Aging Cell* **11**, 491–499 (2012).

39. Brunquell, J., Morris, S., Lu, Y., Cheng, F. & Westerheide, S. D. The genome-wide role of HSF-1 in the regulation of gene expression in Caenorhabditis elegans. *BMC Genomics*

17, 1–18 (2016).

40. Watts, J. L. & Ristow, M. Lipid and Carbohydrate Metabolism in Caenorhabditis elegans. *Genetics* **207**, 413–446 (2017).

41. Watts, J. L. & Browse, J. A palmitoyl-CoA-specific delta9 fatty acid desaturase from Caenorhabditis elegans. *Biochem. Biophys. Res. Commun.* **272**, 263–269 (2000).

42. Imanikia, S., Sheng, M., Castro, C., Griffin, J. L. & Taylor, R. C. XBP-1 Remodels Lipid Metabolism to Extend Longevity. *Cell Rep.* **28**, 581-589.e4 (2019).

43. Castillo-Quan, J. I. *et al.* An antisteatosis response regulated by oleic acid through lipid droplet–mediated ERAD enhancement. *Sci. Adv.* **9**, (2023).

44. Shmookler Reis, R. J. *et al.* Modulation of lipid biosynthesis contributes to stress resistance and longevity of *C. elegans* mutants. *Aging (Albany. NY).* **3**, 125–147 (2011).

45. Papsdorf, K. & Brunet, A. Linking Lipid Metabolism to Chromatin Regulation in Aging. *Trends Cell Biol.* **29**, 97–116 (2019).

46. Gille, B., Galuska, C. E., Fuchs, B. & Peleg, S. Recent Advances in Studying Age-Associated Lipids Alterations and Dietary Interventions in Mammals. *Front. Aging* **2**, 63 (2021).

47. Watterson, A. *et al.* Loss of heat shock factor initiates intracellular lipid surveillance by actin destabilization. *Cell Rep.* **41**, 111493 (2022).

48. Ghisla, S. & Thorpe, C. Acyl-CoA dehydrogenases. *Eur. J. Biochem.* **271**, 494–508 (2004).

49. Ramachandran, P. V *et al.* Lysosomal Signaling Promotes Longevity by Adjusting Mitochondrial Activity. *Dev. Cell* **48**, 685-696.e5 (2019).

50. Piazzesi, A. *et al.* CEST-2.2 overexpression alters lipid metabolism and extends longevity of mitochondrial mutants. *EMBO Rep.* **23**, e52606 (2022).

51. Ratnappan, R. *et al.* Germline Signals Deploy NHR-49 to Modulate Fatty-Acid β-Oxidation and Desaturation in Somatic Tissues of C. elegans. *PLOS Genet.* **10**, e1004829 (2014).

52. Lee, S. K. S. H., Lee, S. K. S. H., Paik, D. & Min, K. J. Overexpression of fatty-acid-β-oxidation-related genes extends the lifespan of drosophila melanogaster. *Oxid. Med. Cell. Longev.* (2012) doi:10.1155/2012/854502.

53. Weir, H. J. *et al.* Dietary Restriction and AMPK Increase Lifespan via Mitochondrial Network and Peroxisome Remodeling. *Cell Metab.* **26**, 884 (2017).

54. Kishimoto, S., Uno, M., Okabe, E., Nono, M. & Nishida, E. Environmental stresses induce transgenerationally inheritable survival advantages via germline-to-soma communication in Caenorhabditis elegans. *Nat Commun* **8**, 14031 (2017).

55. Nono, M. *et al.* Intestine-to-Germline Transmission of Epigenetic Information Intergenerationally Ensures Systemic Stress Resistance in C. elegans. *Cell Rep* **30**, 3207-3217 e4 (2020).

56. Obata, F., Fons, C. O. & Gould, A. P. Early-life exposure to low-dose oxidants can increase longevity via microbiome remodelling in Drosophila. *Nat Commun* **9**, 975 (2018).

57. Kennedy, B. K. *et al.* Geroscience: Linking Aging to Chronic Disease. *Cell* **159**, 709–713 (2014).

58. Labbadia, J. & Morimoto, R. I. Repression of the Heat Shock Response Is a Programmed Event at the Onset of Reproduction. *Mol. Cell* (2015) doi:10.1016/j.molcel.2015.06.027.

59. Lee, D. *et al.* MDT-15/MED15 permits longevity at low temperature via enhancing

lipidostasis and proteostasis. *PLOS Biol.* **17**, e3000415 (2019).

60. Steinbaugh, M. J. *et al.* Lipid-mediated regulation of SKN-1/Nrf in response to germ cell absence. *Elife* **4**, (2015).

61. Goudeau, J. *et al.* Fatty Acid Desaturation Links Germ Cell Loss to Longevity Through NHR-80/HNF4 in C. elegans. *PLOS Biol.* **9**, e1000599 (2011).

62. Schroeder, E. A. & Brunet, A. Lipid Profiles and Signals for Long Life. *Trends Endocrinol. Metab.* **26**, 589–592 (2015).

63. Littlejohn, N. K., Seban, N., Liu, C. C. & Srinivasan, S. A feedback loop governs the relationship between lipid metabolism and longevity. *Elife* **9**, 1–26 (2020).

64. Morgan, M. A. J. & Shilatifard, A. Reevaluating the roles of histone-modifying enzymes and their associated chromatin modifications in transcriptional regulation. *Nat. Genet. 2020 5212* **52**, 1271–1281 (2020).

65. Pu, M., Wang, M., Wang, W., Velayudhan, S. S. & Lee, S. S. Unique patterns of trimethylation of histone H3 lysine 4 are prone to changes during aging in Caenorhabditis elegans somatic cells. *PLoS Genet* **14**, e1007466 (2018).

66. Gomez-Pastor, R., Burchfiel, E. T. & Thiele, D. J. Regulation of heat shock transcription factors and their roles in physiology and disease. *Nat. Rev. Mol. Cell Biol. 2017 191* **19**, 4–19 (2017).

67. Brenner, S. The genetics of Caenorhabditis elegans. *Genetics* **77**, 71–94 (1974).

68. Ly, K., Reid, S. J. & Snell, R. G. Rapid RNA analysis of individual Caenorhabditis elegans. *MethodsX* **2**, 59–63 (2015).

69. Livak, K. J. & Schmittgen, T. D. Analysis of relative gene expression data using real-time

quantitative PCR and the 2(-Delta Delta C(T)) Method. *Methods* **25**, 402–408 (2001).

70. Matyash, V., Liebisch, G., Kurzchalia, T. V., Shevchenko, A. & Schwudke, D. Lipid extraction by methyl-tert-butyl ether for high-throughput lipidomics. *J. Lipid Res.* **49**, 1137–1146 (2008).

71. Pang, Z. *et al.* MetaboAnalyst 5.0: narrowing the gap between raw spectra and functional insights. *Nucleic Acids Res.* **49**, W388–W396 (2021).

72. Martin, M. Cutadapt removes adapter sequences from high-throughput sequencing reads. *EMBnet.journal* **17**, 10–12 (2011).

73. Kim, D., Langmead, B. & Salzberg, S. L. HISAT: a fast spliced aligner with low memory requirements. *Nat. Methods 2015 124* **12**, 357–360 (2015).

74. Pertea, M. *et al.* StringTie enables improved reconstruction of a transcriptome from RNA-seq reads. *Nat. Biotechnol. 2015 333* **33**, 290–295 (2015).

75. Love, M. I., Huber, W. & Anders, S. Moderated estimation of fold change and dispersion for RNA-seq data with DESeq2. *Genome Biol.* **15**, 1–21 (2014).

76. Robinson, M. D., McCarthy, D. J. & Smyth, G. K. edgeR: a Bioconductor package for differential expression analysis of digital gene expression data. *Bioinformatics* **26**, 139–140 (2010).

77. Walker, M. D. *et al.* WormPaths: Caenorhabditis elegans metabolic pathway annotation and visualization. *Genetics* **219**, (2021).

78. Escorcia, W., Ruter, D. L., Nhan, J. & Curran, S. P. Quantification of Lipid Abundance and Evaluation of Lipid Distribution in Caenorhabditis elegans by Nile Red and Oil Red O Staining. *JoVE (Journal Vis. Exp.* **2018**, e57352 (2018).

79. Koopman, M. *et al.* A screening-based platform for the assessment of cellular respiration in Caenorhabditis elegans. *Nat. Protoc. 2016 1110* **11**, 1798–1816 (2016).

Fig. 1

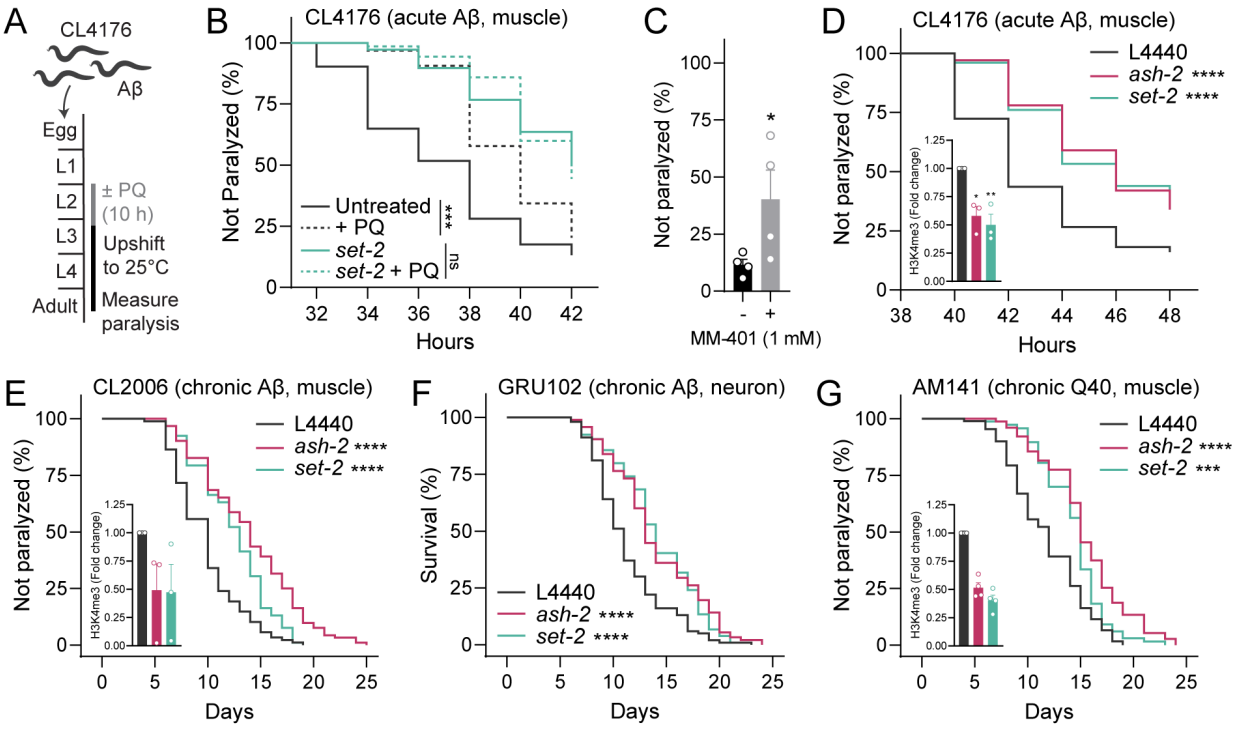

Fig. 1. Disruption of H3K4me3 modifiers protects *C. elegans* against amyloid toxicity
(A) Schematic for PQ treatment of $A\beta_{1-42}$ expressing strain CL4176 in *(B),* where age-synchronized wild-type or *set-2 (ok952)* CL4176 animals were exposed to 1 mM PQ for 10 h during the L2 larval stage and assessed for Aβ-mediated paralysis after temperature upshift. *(C)* CL4176 animals were maintained from egg on either control NGM plates or on plates containing the histone methyltransferase inhibitor MM-401 (1 mM). Paralysis was assessed 40 h post-temperature upshift. *(D)* Paralysis of CL4176 *C. elegans* maintained on bacteria expressing either control (i.e. L4440), *ash-2* or *set-2* RNAi. *(E)* Paralysis of $A\beta_{1-42}$-expressing CL2006 maintained on control (i.e. L4440), *ash-2* or *set-2* RNAi. *(F)* Survival of GRU102 animals (neuronal $A\beta_{1-42}$) maintained on control (i.e. L4440), *ash-2* or *set-2* RNAi. *(G)* Paralysis of Q40::YFP (AM141) *C. elegans* maintained on control (i.e. L4440), *ash-2* or *set-2* RNAi. *(D, E, G insets)* H3K4me3 levels assessed by western blot analysis using Day 1 adults. Total H3 was used as control. Results are representative *(B, D, E-G)* or the average ± SEM *(C, insets in D, E, G)* of two *(F)*, three *(B-E)*, or four *(G)* independent experiments. Detailed information on the number of worms per condition and statistical analysis for biological replicates of paralysis curves is shown in Table S1.

Fig. 2

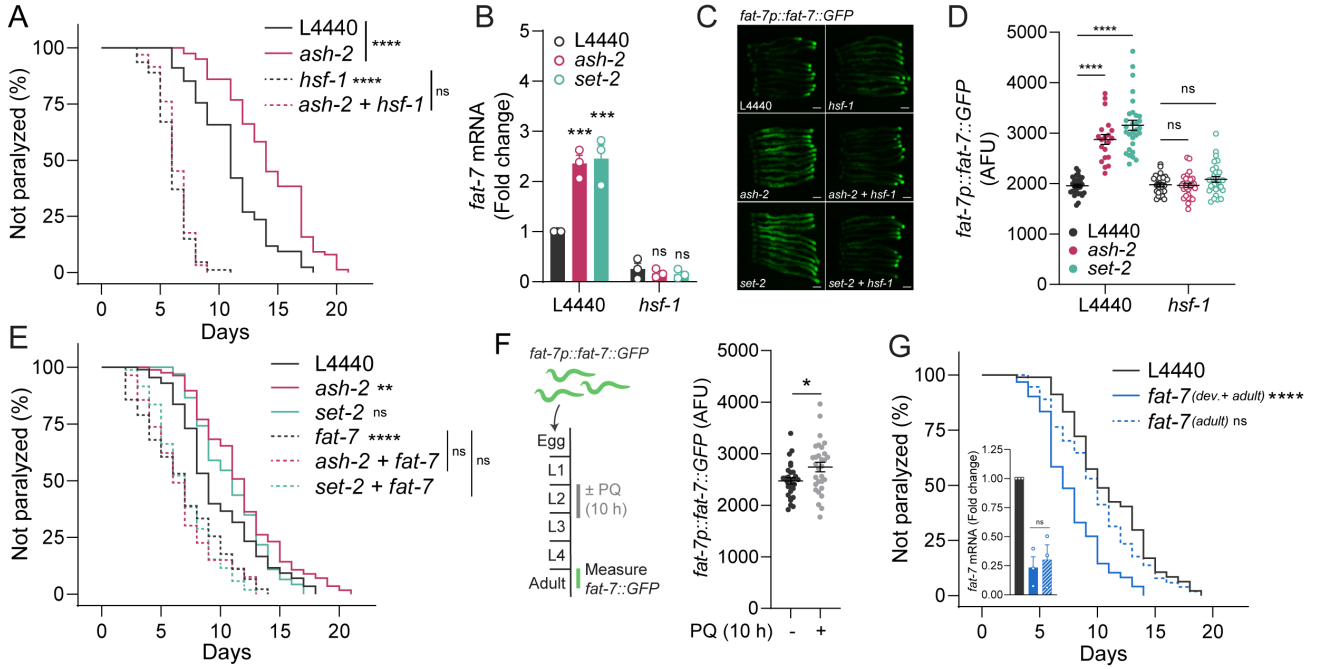

Fig. 2. Protective effect of H3K4me3 depletion is due to HSF-1 mediated FAT-7 upregulation
(A) Paralysis of Q40::YFP *C. elegans* maintained on control (i.e. L4440) or *ash-2* RNAi in the presence or absence of *hsf-1* RNAi. Simultaneous knockdown of *ash-2* with *hsf-1* was achieved by mixing equal amounts of each RNAi bacteria. The resulting dilution of RNAi bacteria under these conditions was accounted for in the other conditions by combining the target gene RNAi with equal amounts of control RNAi encoding L4440 bacteria (knockdown efficiency shown in Fig. S2C). *(B)* Accumulation of *fat-7* mRNA in Q40::YFP animals maintained on control (i.e., L4440), *ash-2 or set-2* RNAi in the presence or absence of *hsf-1* RNAi was assessed by qPCR in day 1 adults and normalized to the house-keeping gene *pmp-3*. *(C, D)* Fluorescence of *fat-7p::fat-7::GFP* expressing *C. elegans* maintained on control (i.e., L4440), *ash-2, set-2, hsf-1, ash-2 + hsf-1 or set-2 + hsf-1* RNAi was measured in day 1 adults (*C*) and quantified (*D*). At least 20 animals were assessed per condition. Scale bar in (C) is 0.1 mm. *(E)* Paralysis of Q40::YFP animals maintained on control (i.e., L4440), *ash-2, set-2, fat-7, ash-2 + fat-7, or set-2 + fat-7* RNAi. (*F)* Quantification of fluorescence of adult *fat-7p::fat-7::GFP* expressing *C. elegans* maintained on OP50 bacteria and exposed to paraquat (PQ, 1 mM) for 10 h during the L2 larval stage. The FAT-7::GFP fluorescence was imaged in day 1 adults. *(G)* Q40::YFP animals were cultivated on control (i.e. L4440) or *fat-7* RNAi starting at the time of egg lay. Worms were then either maintained on *fat-7* RNAi (*dev. + adult*) or shifted from L4440 to *fat-7* RNAi 72 h after egg *(adult*). Inset in *(G)* shows mRNA expression of *fat-7* in animals collected at 96 h after egg, showing a comparable decrease in *fat-7* expression between conditions. Results are representative *(A, C-G)*, average ± SEM (*B, inset in G)* of two *(F),* three *(B-E, G)*, or four *(A)* independent experiments. Statistical significance was assessed by log-rank *(A, E, G)*, one-way ANOVA *(B, inset in G),* Kruskal-Wallis test *(D)* or Mann-Whitney test *(F)*; *, $p<0.05$; **, $p<0.01$; ***, $p<0.001$; ****, $p<0.0001$. Additional experimental information, paralysis statistics, and data for biological replicates can be found in Table S1.

Fig. 3

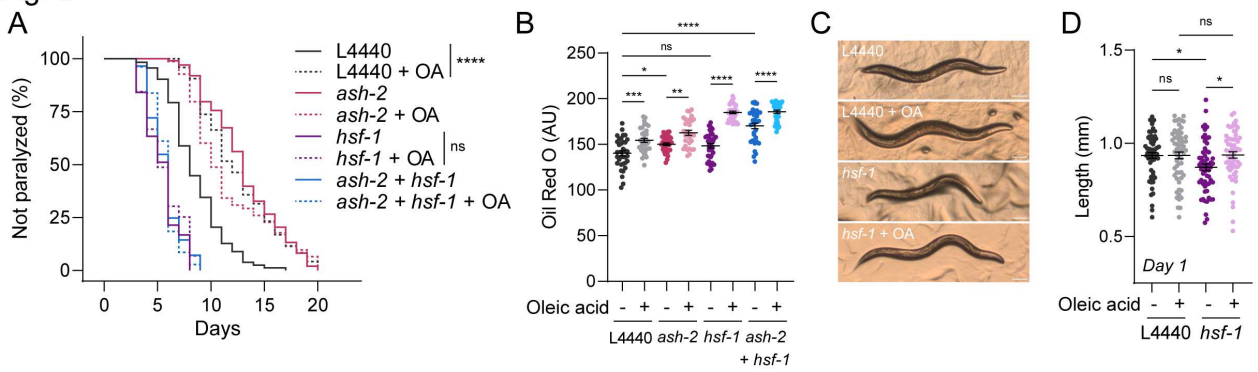

Fig. 3. Oleic acid protects against proteotoxicity in an HSF-1-dependent manner
(A) Q40::YFP animals were synchronized by timed egg lay on L4440, *ash-2, hsf-1*, or *ash-2* + *hsf-1* seeded NGM plates with or without supplementation with oleic acid (0.8 mM), and paralysis was examined. *(B)* Quantification of fat content under conditions in *(A)* with Oil red O staining at day 1 of adulthood. *(C)* Representative images of day 1 adult Q40::YFP animals maintained on L4440 or *hsf-1* RNAi ± oleic acid *(A),* and quantification of animal size in *(D)*. A minimum of 30 animals were assessed per condition. Scale bar is 0.1 mm. Results are representative *(A-D)* of two *(A)* or three *(B-D)* independent experiments. Statistical significance was assessed by log-rank *(A)* or Kruskal-Wallis *(B, D)*; $p<0.05$, *; $p<0.01$, **; $p<0.001$, ***; $p<0.0001$, ****. Additional experimental information, and data for biological replicates not shown, can be found in Table S1.

Fig. 4

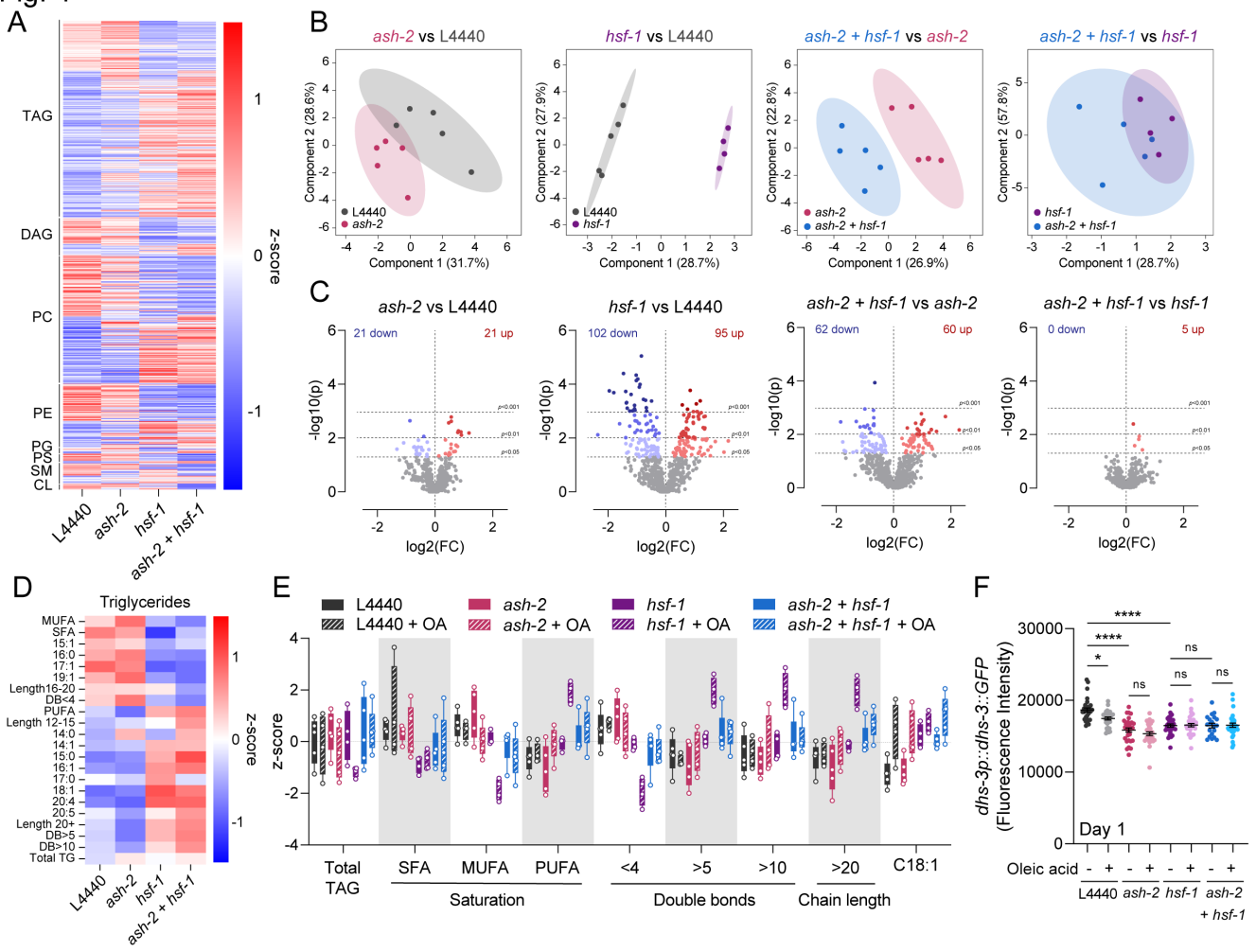

Fig. 4. Disruption of HSF-1 remodels the lipid landscape

(A) Heat map of lipid species detected by mass spectrometry in day 1 adult Q40::YFP animals maintained on L4440, *ash-2*, *hsf-1*, or *ash-2* + *hsf-1* RNAi bacteria. Values represent the average z-score from 4-5 biological replicates. TG, triacylglyceride; DAG, diacylglyceride; PC, phosphatidylcholine; PE, phosphatidylethanolamine; PG, phosphatidylglycerol; PS, phosphatidylserine; SM, sphingomyelin; CL, cardiolipin. *(B)* Partial least squares-discriminant analysis (PLS-DA) plots of individual samples from conditions in *(A)*. *(C)* Volcano plots of differentially expressed lipids under indicated RNAi conditions and comparisons. *(D)* Heat map and *(E)* z-score plot of triglyceride composition features in Q40::YFP animals maintained under conditions in *(A)* with and without oleic acid supplementation. *(F)* Quantification of lipid droplet fluorescence in day 1 adult *dhs-3p::dhs-3::GFP C. elegans* maintained on conditions in *(A)*. Results are the average *(A, D, E)* or representative *(F)* of at least four *(A-E)* or three biological *(F)* replicates. Statistically significant differences were determined by one-way ANOVA; *, p<0.05; ****, p<0.0001. Additional information on lipidomics data can be found in Table S3.

Fig. 5

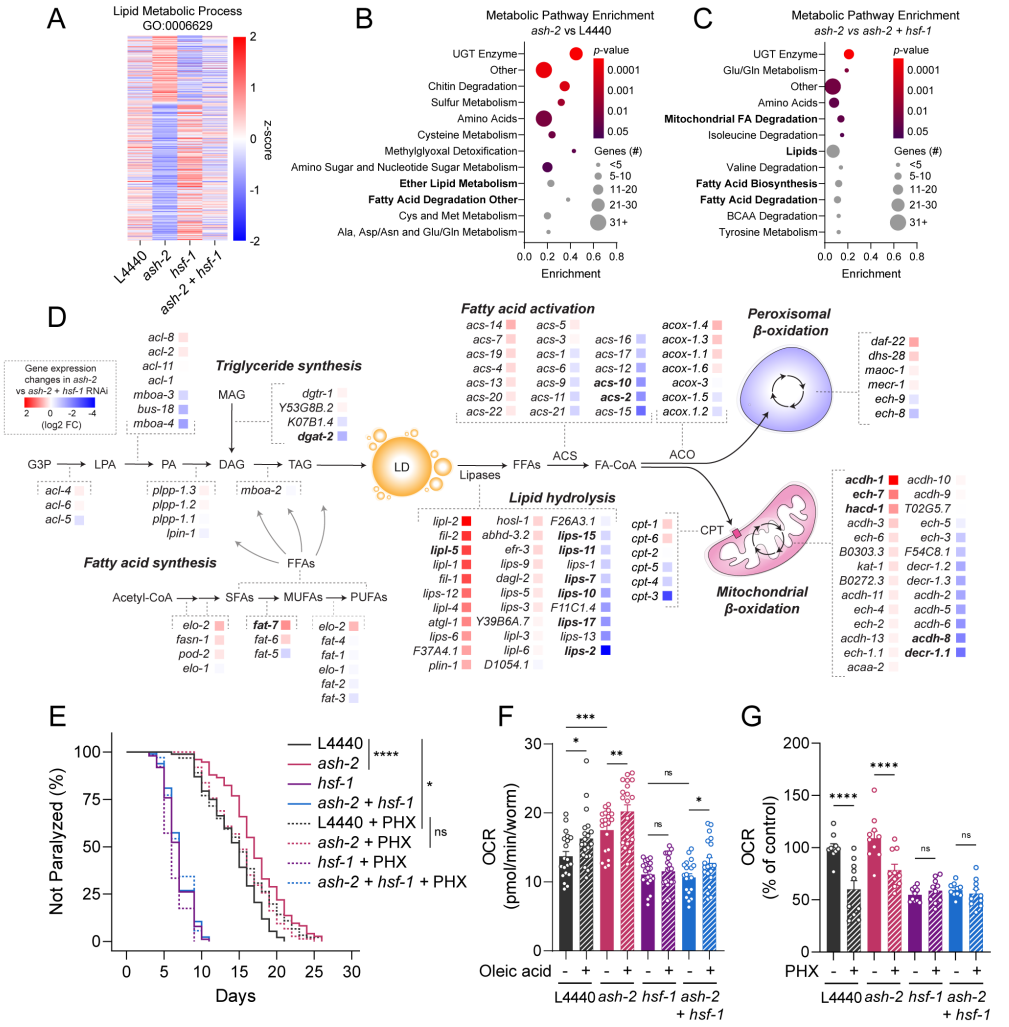

Fig. 5. Differential regulation of lipid metabolism by *hsf-1* governs resistance to proteotoxicity in the absence of *ash-2*. *(A)* Heat map of expression changes in genes involved in lipid metabolic processes (GO:0006629) in day 1 adult Q40::YFP worms maintained on L4440, *ash-2*, *hsf-1*, or *ash-2* + *hsf-1* RNAi. Values are the average z-score from 4-5 biological replicates. *(B-C)* Metabolic pathway enrichment analysis (WormFlux) of differentially expressed genes between *ash-2* vs L4440 *(B)* or *ash-2* + *hsf-1* vs *ash-2 (C)*. Categories with a *p*-value <0.05 were considered enriched and colored according to the scale, and categories with a *p*-value >0.05 colored gray. *(D)* Expression changes of genes involved in fatty acid synthesis and degradation in day 1 adult Q40::YFP worms maintained on *ash-2* + *hsf-1* RNAi *versus ash-2* RNAi. Statistically significant changes are depicted in bold. *(E)* Paralysis of Q40::YFP worms maintained on L4440, *ash-2*, *hsf-1*, or *ash-2* + *hsf-1* RNAi bacteria in the presence or absence of perhexiline (PHX). *(F)* Oxygen consumption rates (OCRs) of day 1 adult Q40::YFP worms maintained on L4440, *ash-2*, *hsf-1*, or *ash-2* + *hsf-1* RNAi ± oleic acid (0.8 mM) measured using a Seahorse XFe96 analyzer. Five baseline OCR measurements were taken per experiment, with each point representing the average baseline OCR reading of 3-5 technical replicate wells across four independent experiments. Wells containing fewer than 5 worms were excluded from the analysis. *(G)* OCR in day 1 Q40::YFP worms maintained on L4440, *ash-2*, *hsf-1*, or *ash-2* + *hsf-1* RNAi ± perhexiline (2.5 mM). Results are the average *(A, D),* average ± SEM *(F-G)* of two *(G)* or at least three *(A-F)* independent experiments. Statistically significant differences were assessed by log-rank *(E)* or one-way ANOVA *(F, G)*; *, p<0.05; **, p<0.01; ****, p<0.0001. Data for biological replicates not shown can be found in Table S1, and detailed experimental information for RNAseq analysis can be found in Table S2.

Fig. 6

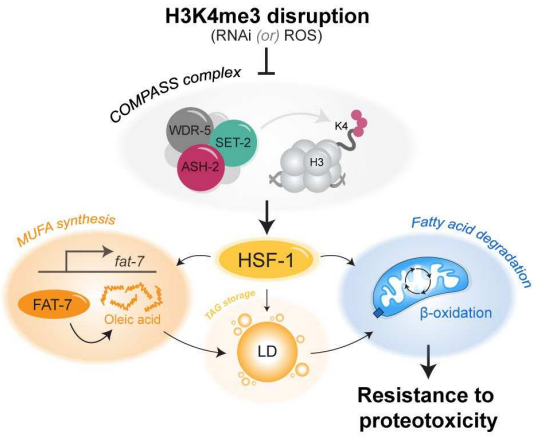

Fig. 6. Working model
Proposed mechanism by which early-in-life inactivation of H3K4me3-modifiers protects against proteotoxicity later in life. Depletion of H3K4me3 leads to the upregulation of HSF-1 activity, which is essential for the protective effect displayed by H3K4me3-deficient worms. HSF-1 activity is required for the upregulation of FAT-7, an enzyme which converts stearic acid into oleic acid, a protective mono-unsaturated fatty acid (MUFA). Although production of oleic acid is necessary for the observed protection, it's presence is insufficient to delay the onset of amyloid toxicity. HSF-1 mediated stimulation of mitochondrial β-oxidation is required to fully protect against amyloid-mediated paralysis. Previous studies and our work showed that the activities of H3K4me3-modifiers, HSF-1 and FAT-7 in early life are directly linked to their protective effects later in life. It remains to be tested precisely how changes in lipid homeostasis protect against proteotoxicity.

Supplementary Files

This is a list of supplementary files associated with this preprint. Click to download.

- NatAgingOlesonSupplement.pdf